Available online at www.sciencedirect.com
SCIENCE DIRECT®
European Journal of Mechanics B/Fluids 23 (2004) 229–239

Predicted low frequency structures in the wake of elliptical cylinders

Shaun A. Johnson *, Mark C. Thompson, Kerry Hourigan

Fluids Laboratory for Aeronautical and Industrial Research (FLAIR), Department of Mechanical Engineering, Monash University, Clayton, Victoria, 3800 Australia

Received 14 April 2003; accepted 27 May 2003

Abstract

The vortex structures in the wake of 2D elliptical cylinders at low Reynolds numbers are investigated for a Reynolds numbers range of 75 to 175 using direct numerical simulation. By varying the aspect ratio of an elliptical cylinder, the geometry is varied between the extremes of a circular cylinder and a flat plate normal to the flow. The power spectrum analysis of the vertical velocity along the horizontal centreline shows the presence of secondary and tertiary frequencies in the far region of the wake. As the Reynolds number is increased and/or the aspect ratio is decreased, the lower frequencies in the far wake become more dominant and their inception point occurs closer to the elliptical cylinder. This research suggests that the low frequency unsteadiness behind normal flat plates does not need to be due to the vortex interaction, but, rather, can result from the presence of a two-dimensional instability of the mean wake.

Keywords: Elliptical cylinder; Low frequency unsteadiness; Far wake; Low Reynolds numbers

1. Introduction

Flow structures behind bluff bodies have been the focus of extensive research due to, amongst other things, their importance to the drag on vehicles and structures. The circular cylinder has been the generic bluff body used for the majority of research. However, at low Reynolds numbers (Re), the low frequency unsteadiness that is observed behind normal flat plates is not present in the near wake. In the present study, the use of elliptical cylinders will be shown to facilitate the numerical analysis of large structures that occur in the far wake because they form closer to the body before they are diffused.

Najjar and Balachandar [1] conducted both two-dimensional (2D) and three-dimensional (3D) simulations on a normal flat plate at $Re = 250$ and investigated low frequency unsteadiness. In the 2D simulations, the drag coefficient exhibited a dominant periodic cycle driven by the shedding of von Karman type vortices. However, a low frequency component was apparent in the time history of the drag coefficient. Najjar and Balachandar stated that the Karman vortex interaction downstream caused the low frequency unsteadiness. In the 3D simulations, the drag history showed a more unpredictable periodicity. The mechanism responsible for the low frequency unsteadiness was due to a gradual switching back and forth between shedding cycles of high mean and low mean drag. The high-drag regime wake resembled a mode B-type wake structure [2], while the low-drag regime wake resembled a flow similar to that caused by large-scale dislocation, both similar to states observed behind circular cylinders [3]. The 2D simulations were largely ignored by Najjar and Balachandar, even though low-frequency unsteadiness was present, because the wake structures were so different from the 3D results.

* Corresponding author.
E-mail address: shaun.johnson@eng.monash.edu.au (S.A. Johnson).

0997-7546/$ – see front matter
doi:10.1016/j.euromechflu.2003.05.006

Few studies have explored flow structures in the far wake that are different from those observed in the near wake region. Visualisations made by Taneda [4] showed the decay of the Karman street wake and the growth of a larger secondary structure in the far wake that appeared to be much like the original Karman vortex street, but with a longer wavelength. Taneda concluded that the secondary vortex street was due a hydrodynamic instability based on the mean velocity profile. It was supposed that the original wake structure decays and the wake 'rearranges' itself into a new configuration appropriate to the changed conditions downstream. Cimbala et al. [5] concluded that the secondary wake structure did not depend on the scale or frequency of the Karman shedding frequency. Rather, their results showed that the frequencies amplified in the far wake were not related to the Karman shedding frequency but had good agreement to those found using linear stability theory. Conversely, Williamson [6] demonstrated that the near wake (F_K) frequency directly influenced the far wake. The frequency of the far wake (F_{FW}) was given by $F_{FW} = F_K - F_T$ where F_T was the frequency of the two-dimensional instability. He also showed that the far wake was extremely sensitive to free-stream disturbances. As a result of this sensitivity, it was very difficult to define a natural wake state.

This paper examines the nominally two-dimensional wake states behind elliptical bodies at low Reynolds numbers using numerical simulation as the body geometry is changed from a flat plate normal to the free stream flow to that of a circular cylinder. In particular, it is concerned with secondary and tertiary structures in the wake and their associated frequencies. A parameter space model for the wake structures (revised from [7]) is outlined and the power spectra are analysed.

The two parameters that were varied in this investigation were the Aspect Ratio (AR) and Reynolds number (Re). Shown in Fig. 1 is the progression of a normal flat plate ($AR = 0$) to a cylinder ($AR = 1$). The transverse width (A) is used as the Re length scale for the simulations.

A 2D spectral-element method was used to solve the unsteady Navier–Stokes equations governing the fluid flow. The spectral-element method is based on the Galerkin finite-element method incorporating high-order Lagrangian polynomial shape functions within each element. This method has been validated in many simulations, and especially on circular cylinder wakes [8]. Simulations were carried out for $AR = 0.01$ to 1.00 and for $Re = 75$ to 175.

The macro grid employed is displayed in Fig. 2. The origin of the axis is located at the centre of the cylinder. To accommodate different aspect ratio elliptical bodies, the grid near the cylinder was stretched. The same number of macro-elements was used near the surface of the ellipse to capture the boundary layer. A boundary condition of uniform velocity was assigned to the top and bottom edges, and on the circular left boundary. The side boundaries were positioned $30A$ away from the cylinder. The

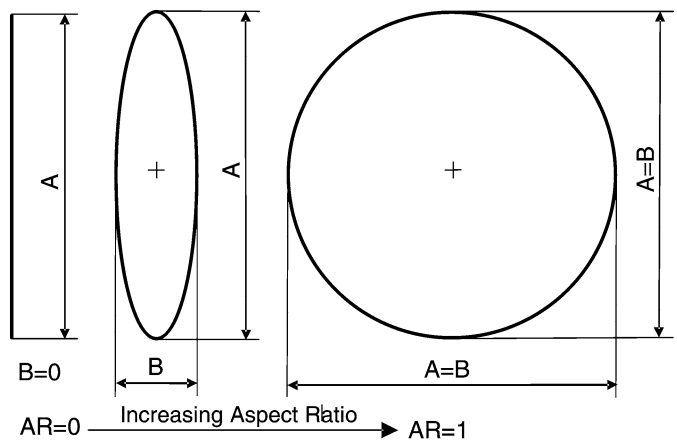

Fig. 1. Schematic diagram of changing aspect ratio. Shown is $AR = 0.01$, $AR = 0.25$, and $AR = 1.0$.

Table 1
Dependence of Strouhal number and mean drag coefficient on the polynomial order for $AR = 0.25$ at $Re = 175$

Element size ($N \times N$)	Strouhal number	Mean Cd
5×5	0.16822	1.0896
6×6	0.16585	1.0716
7×7	0.16542	1.0689
8×8	0.16529	1.0678
9×9	0.16524	1.0675

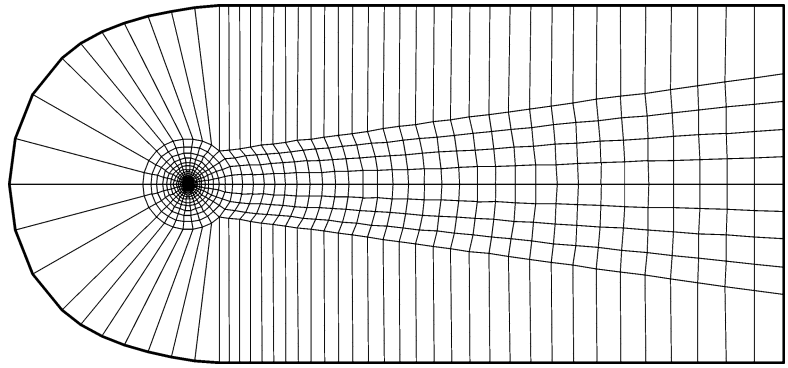

Fig. 2. Macro element grid used for numerical simulations for $AR = 0.25$.

right-hand boundary was specified as an outlet (zero normal velocity gradient condition) and placed $100A$ downstream. The ellipse was specified as a no-slip wall, with the curvature of the walls calculated to produce a smooth surface for the elements used in the spectral-element numerical code.

The resolution of the grid was investigated for $AR = 0.25$ to ensure grid independence. The effect of changing the number of nodes per element in each direction (N) is shown in Table 1. Each macro-element shown in Fig. 2 is subdivided internally into $N \times N$ nodes for the interpolating polynomials (polynomial order is $N - 1$). For the resolution study conducted at $Re = 175$ for $AR = 0.25$, the Strouhal number (St) and drag coefficient on the elliptical cylinder had converged to better than 0.1% by $N = 8$. This accuracy was deemed to be sufficient and $N = 8$ was used for all simulations.

2. Results

2.1. Data collection method

To analyse the frequency response of the flow, simulations were run for 1200 non-dimensional time units until all transient effects were removed from the domain. Time was non-dimensionalised by the upstream velocity and ellipse diameter A. A time history of the X and Y velocity components at 46 discrete points behind the elliptical cylinder on the horizontal centreline was logged for a further 700 non-dimensional time units. This was sufficient to capture at least 6 cycles of the lowest Strouhal period of interest and to conduct a 2^{18} point Fast Fourier Transform (FFT). The power spectrum from the time series of the Y component of velocity was used to determine the dominant frequencies present in the wake as a function of the downstream position.

2.2. Shedding patterns

The six shedding patterns previously outlined by Johnson et al. [7] have been remapped to represent five different flow patterns which have clear boundaries according to the power spectrum along the centreline. These are categorised as the no frequency (F0), primary frequency (F1), secondary frequency with no interaction (F2NI), secondary frequency (F2) and low frequency (LF) regimes. The F0 regime is not discussed in this paper, as there is no associated shedding frequency but is discussed in Johnson et al. [7]. Vorticity plots are used to visualise the wake structures. It must be stressed that the wake development is categorised according to what is observed in the first 100 ellipse widths downstream; it is probable in some cases that the wake evolves different characteristics further downstream. For example, the circular cylinder is known to develop secondary structures hundreds of diameters downstream [5].

The F1 regime corresponds to the standard Karman-type vortex shedding pattern in the wake of the cylinder. As shown in Fig. 3, in the far wake region, positive and negative vortex cores from the primary shedding diffuse together into two rows extending downstream to the outlet. These two shear layers are symmetric about the horizontal centreline.

In the F2NI regime, a two-dimensional instability is apparent in the far wake from the power spectra analysis but it is not visible in vorticity plots (Fig. 4). In the downstream region where the secondary frequency is present, the primary shedding from the cylinder has decayed sufficiently such that it does not interact directly with the vortices from the cylinder and no secondary structures are observed. The flow field visualisations are the similar to those for the F1 regime (Fig. 3) except the breakdown of the primary wake occurs further upstream.

In the F2 region, the two-dimensional instability that is present in the far wake is stronger and the initiation point is occurring further upstream. As a result, a secondary vortex pattern is visible in the wake (Fig. 5) which is due to the increase in strength of

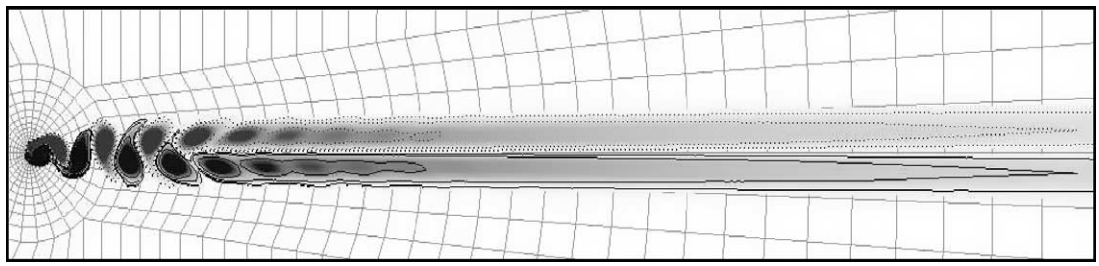

Fig. 3. Vorticity plot of the primary frequency (F1) regime at $Re = 75$ for $AR = 0.25$. The only vortices present are those shed from the cylinder developing into a parallel shear layer in the far wake. The contour range is $(-1, 1)$ with solid lines solid lines indicating regions of positive vorticity and dashed lines indicating negative vorticity. Flow is from left to right.

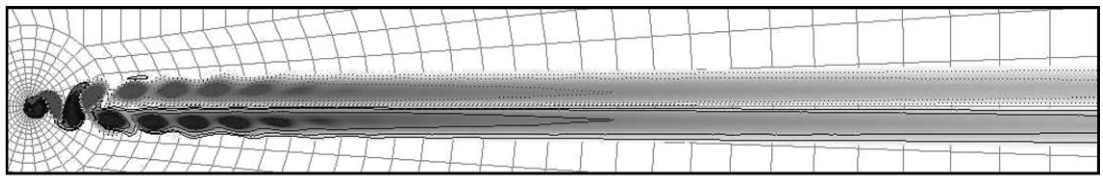

Fig. 4. Vorticity plot of the secondary frequency with no interaction (F2NI) regime at $Re = 100$ for $AR = 0.25$. No secondary structures are visible in the far wake.

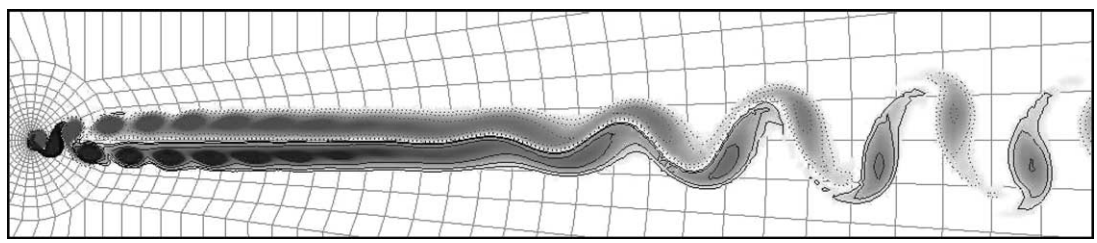

Fig. 5. Vorticity plot of the secondary frequency (F2) regime at $Re = 125$ for $AR = 0.25$. The primary structure breaks down to form a secondary structure in the far wake.

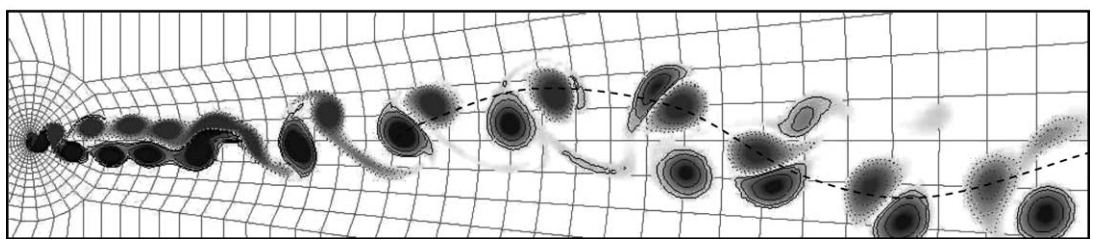

Fig. 6. Vorticity plot of the low frequency (LF) regime at $Re = 175$ for $AR = 0.25$. The primary structure develops into an unsteady structure with a low frequency component present. Note that numerical domain in vertical direction extended well beyond that shown.

the two-dimensional instability. It is important to note that the secondary structure is not a period-doubling mode of the Karman vortex street.

An instantaneous plot of the vorticity in low frequency (LF) regime is shown in Fig. 6. This regime is defined by the presence of a low frequency signal in the power spectrum analysis. The flow structures are quite complex, showing several distinct features. In the near wake region, the Karman vortex street is quickly transformed into an unsteady secondary wake with merging and pairing of the primary vortices where a secondary lower frequency is dominant. At higher Reynolds numbers ($Re > 150$ for $AR = 0.25$), a tertiary frequency dominates the far wake flow field. Flow visualisation animations suggest that the secondary vortex structures start to interact to form a larger structure encompassing the smaller vortices in the region where the tertiary frequency is dominant. However, since the tertiary structures are so close to the outlet, grid domain resolution studies are being undertaken to determine the effect of the outflow boundary condition.

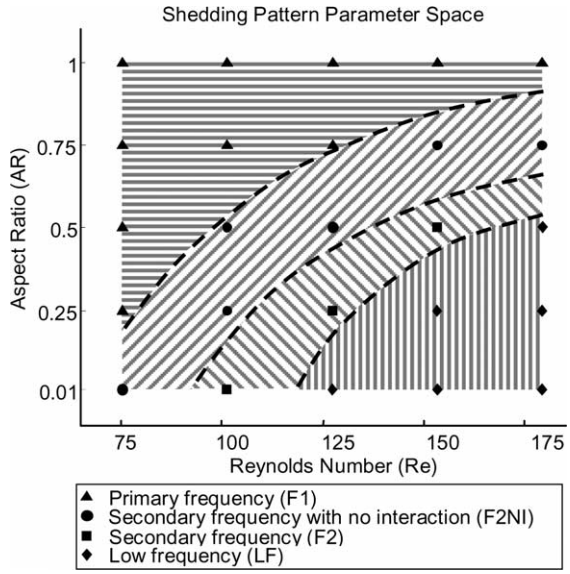

Fig. 7. Shedding pattern parameter space map. Solid lines are included to aid visualisation of boundaries of regimes but do not denote sharp boundaries.

The corresponding wavelength of the low frequency signal is visualised in Fig. 6 by a dashed line passing through the vortex pairs in the wake. This low frequency is due to the interaction of the primary frequency and secondary frequencies as shown by the frequency analysis later.

2.3. Parameter space map

The parameter space model depicting the regions where various regimes occur is shown in Fig. 7. For high *AR* and low *Re*, the F1 regime is present in the wake. As the *AR* decreases and/or the *Re* increases, the wake moves through the F2NI regime until the secondary frequency interacts with the primary frequency in the F2 regime. For high *Re* and low *AR*, the low-frequency structure is present causing unsteady secondary and tertiary structures. Since the outlet boundary is located $100A$ downstream, any frequencies amplified past $100A$ are not included in this parameter space map.

3. Power spectrum analysis

The wake transition that results from the *Re* increase and/or the *AR* decrease is associated with a change in the dominant frequencies present in the wake. The frequencies for a particular aspect ratio, $AR = 0.25$ will be examined below to investigate the flow changes that occur from the F1 to the LF regime as the *Re* is increased (see Figs. 8–17). For each Re, two figures are displayed. The first figure shows the normalised power spectra of the transverse component of the centreline velocity at various locations in the wake. The elliptical cylinder is located at $X/D = 0$ on the centreline distance axis. At each cut downstream, the normalised power amplitude is plotted against the normalised frequency or Strouhal number (*St*). The frequencies of interest (mainly the dominant frequencies) are indicated by vertical shaded planes in the downstream direction. The energy of the frequencies is displayed in the second figure showing their growth and decay as they travel downstream. The energy was calculated by integrating the power of the frequency peaks.

As shown in Fig. 8, at $Re = 75$ (F1 regime), only one frequency is present. This frequency is the primary frequency of the Karman vortex shedding from the elliptical cylinder. The energy decays quickly as the vortices diffuse (Fig. 9) with little energy left in this frequency at $X > 50$.

At $Re = 100$ (F2NI regime), a second frequency corresponding to the two-dimensional instability is present in the far wake, and the power of this instability increases as it propagates downstream (Fig. 10). However, the vortex structures shed from the elliptical cylinder have diffused before onset of the two-dimensional instability. This is shown in Fig. 11 where the energy corresponding to the primary frequency has decayed to the extent where there is no effective energy left before the onset of the secondary mode. No secondary shedding is visible in the vorticity plots from the interaction of the vortex street from the cylinder with the two-dimensional instability.

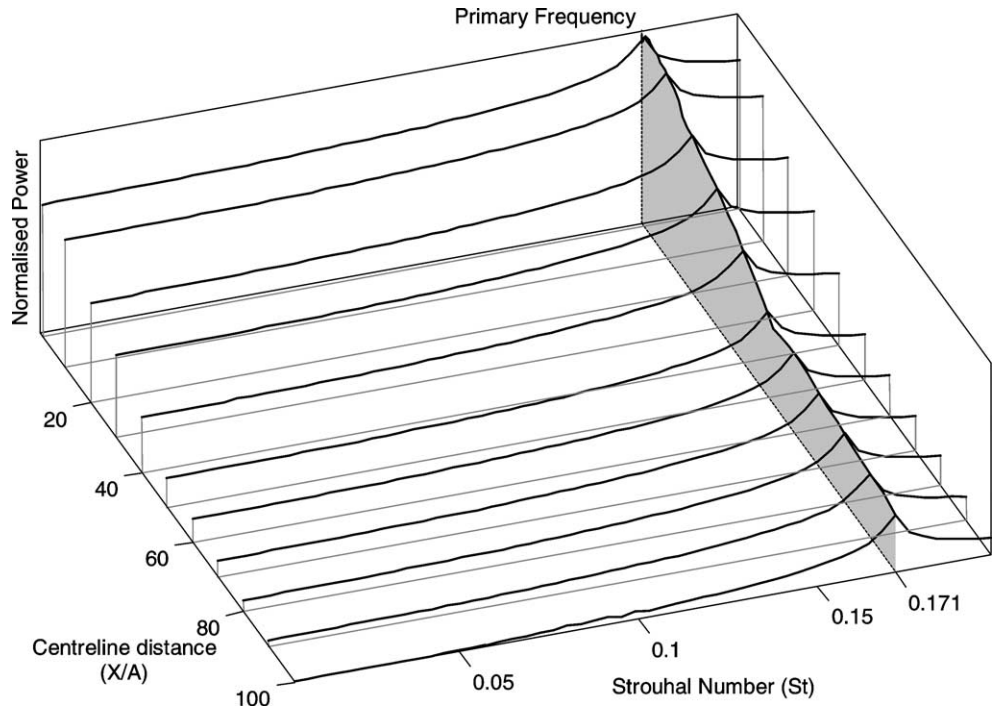

Fig. 8. Normalised power spectra of the transverse velocity component on centreline for $AR = 0.25$ at $Re = 75$.

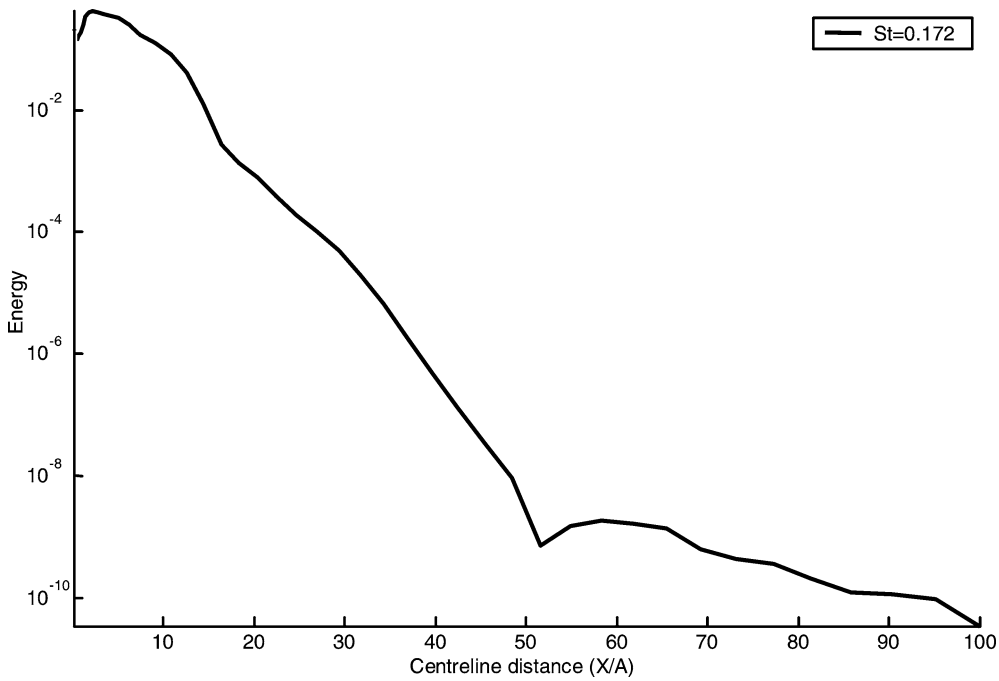

Fig. 9. Downstream development of selected frequency energy for $AR = 0.25$ at $Re = 75$.

In the F2 Regime at $Re = 125$ (Fig. 13), there is increased energy in the secondary instability and substantial amplification occurs further upstream. The secondary structure is periodic which can be seen by the absence of other non-harmonic frequencies in the far wake shown in Fig. 12. The frequency at $St = 0.2004$ is a harmonic of the secondary frequency. The

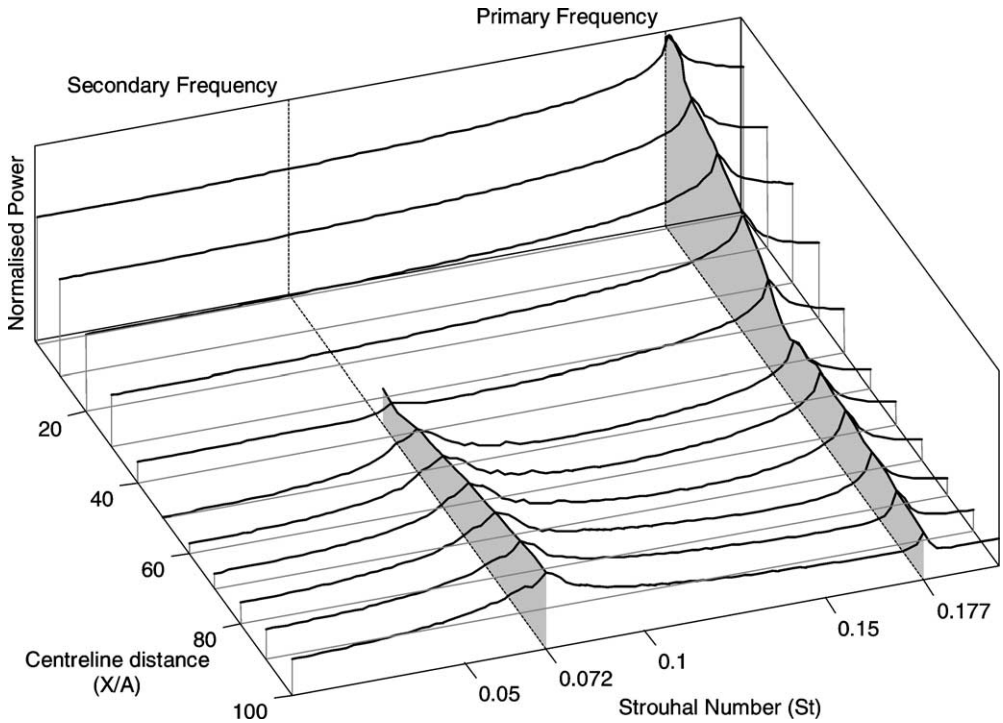

Fig. 10. Normalised power spectra of the transverse velocity component on centreline for $AR = 0.25$ at $Re = 100$.

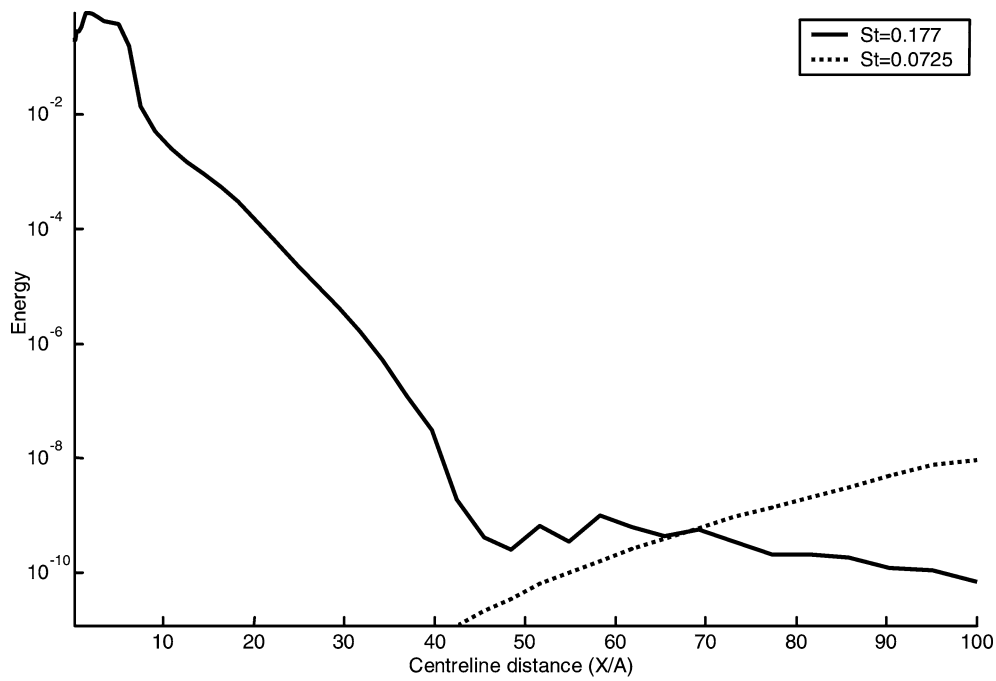

Fig. 11. Downstream development of selected frequency energy for $AR = 0.25$ at $Re = 100$.

secondary structure is not a multiple of the primary frequency suggesting that secondary structure is due to an instability based on the mean velocity profile and is not due to vortex pairing. This secondary instability causes the two parallel rows of vortices to become unstable and start to oscillate. As this new structure moves downstream, it develops into a larger scale vortex street.

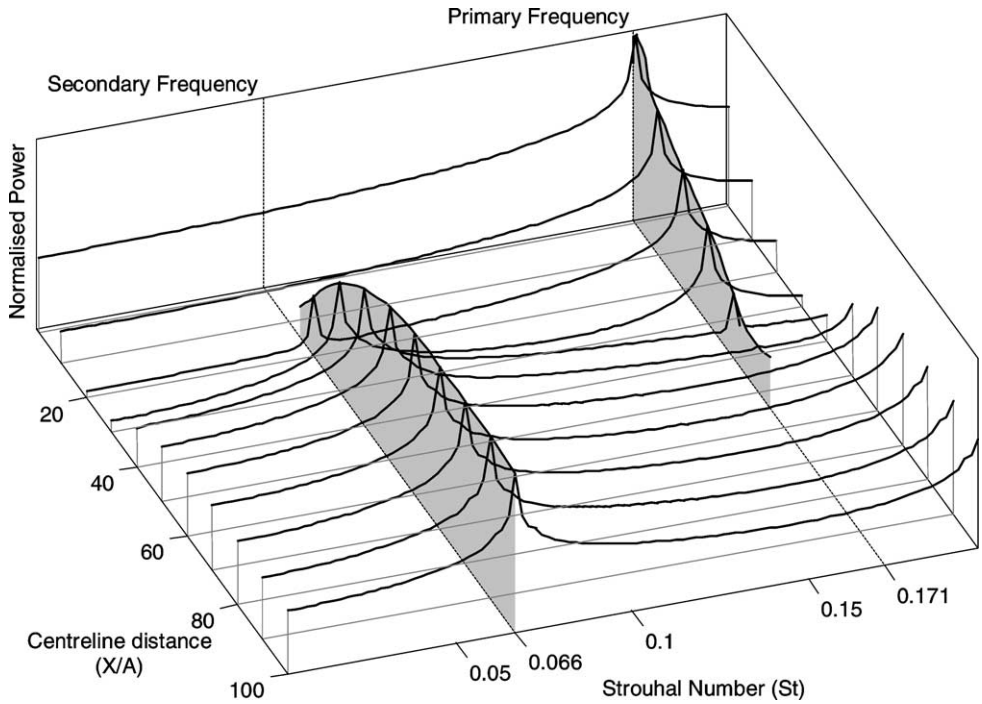

Fig. 12. Normalised power spectra of the transverse velocity component on centreline for $AR = 0.25$ at $Re = 125$.

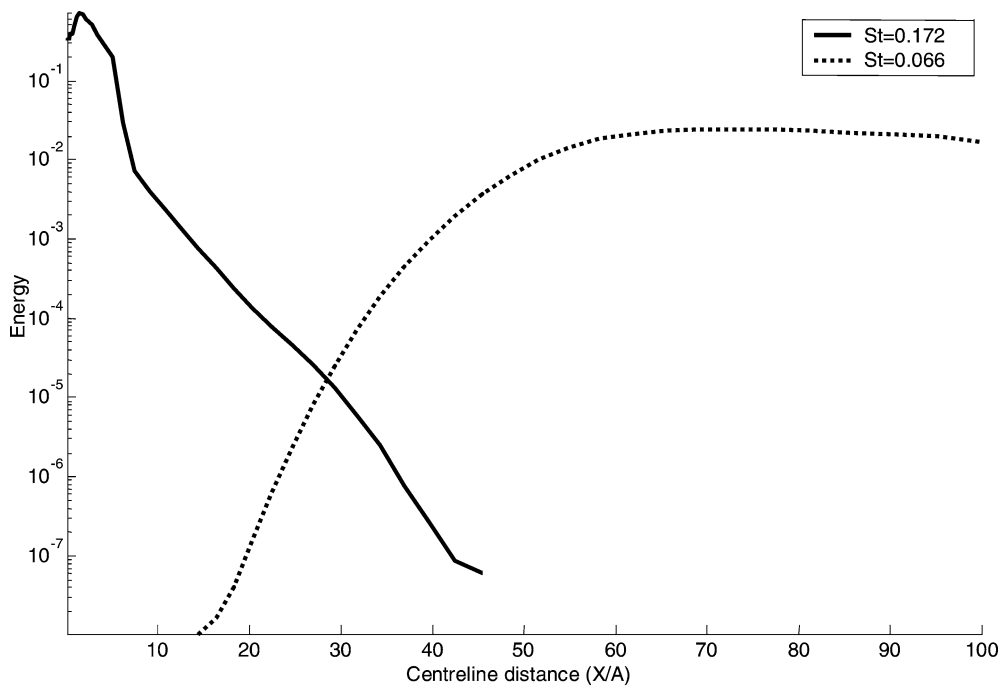

Fig. 13. Downstream development of selected frequency energy for $AR = 0.25$ at $Re = 125$.

When the *Re* is increased to 150, a low frequency component is present in the wake. The normalised power spectra (Fig. 14) shows that the wake is no longer periodic with the *St* content being more chaotic than in the F2 regime. This low frequency appears to be due to the interaction between the primary frequency and secondary frequency. It is not the cause of the secondary

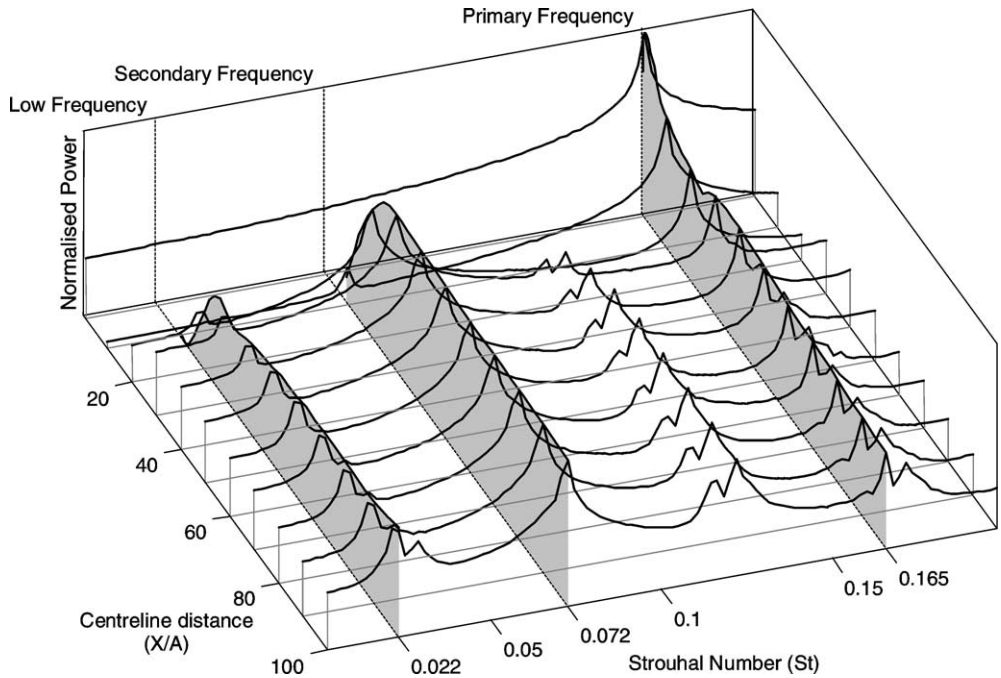

Fig. 14. Normalised power spectra of the transverse velocity component on centreline for $AR = 0.25$ at $Re = 150$.

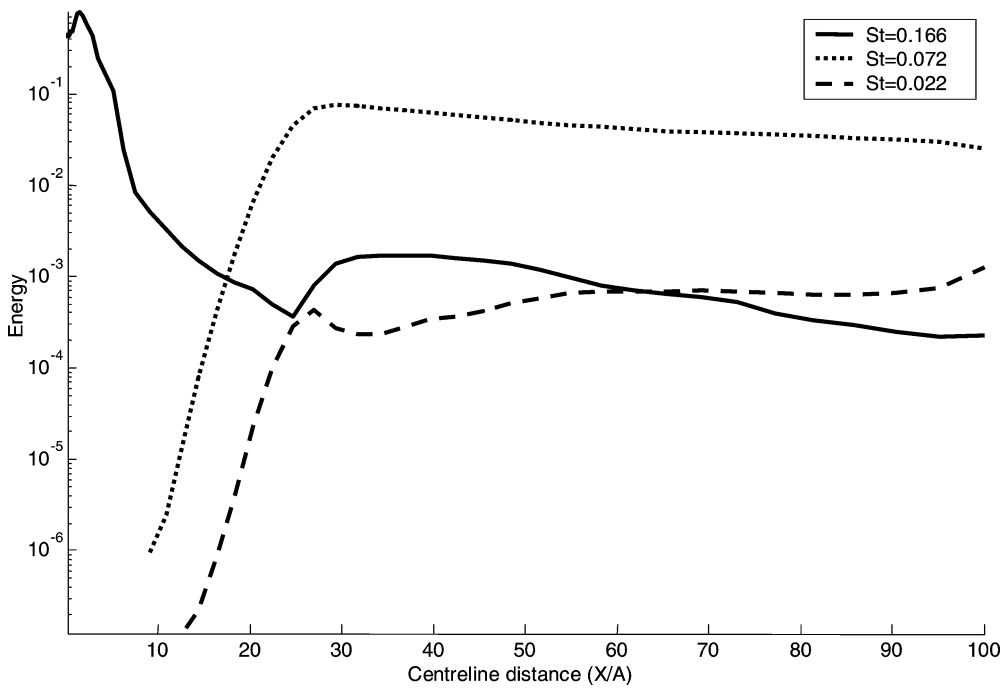

Fig. 15. Downstream development of selected frequency energy for $AR = 0.25$ at $Re = 150$.

shedding since it was not present at lower *Re* and also because the low frequency grows after the secondary shedding frequency has grown as seen in Fig. 15. It is still unclear why this low frequency component is only present at the higher *Re*. The secondary frequency onset is closer to the cylinder and the energy is fairly constant as the structures move downstream.

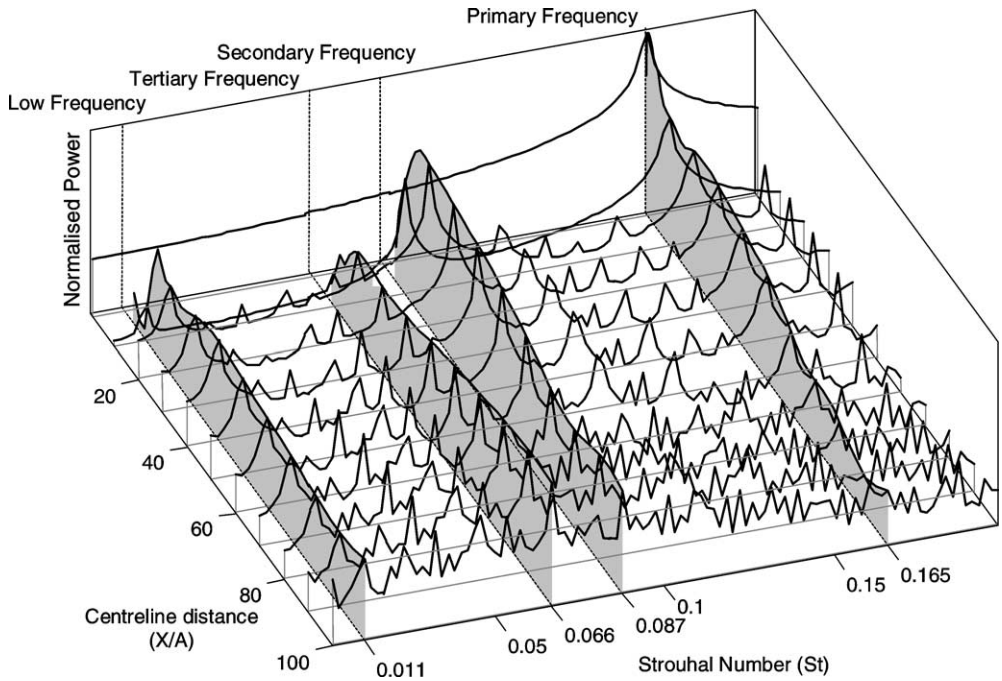

Fig. 16. Normalised power spectra of the transverse velocity component on centreline for $AR = 0.25$ at $Re = 175$.

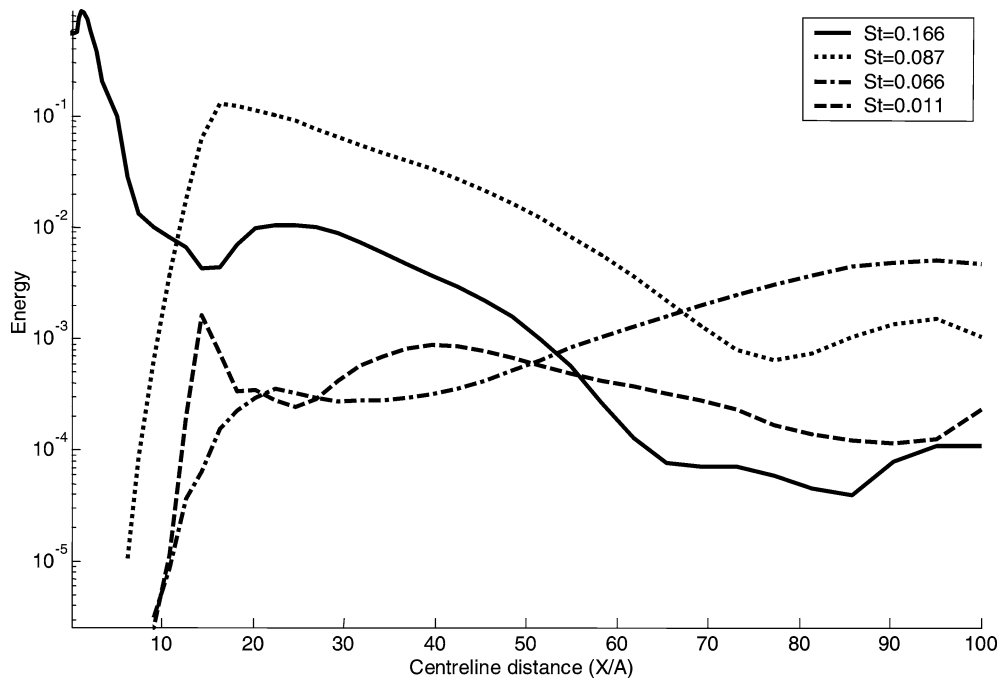

Fig. 17. Downstream development of selected frequency energy for $AR = 0.25$ at $Re = 175$.

Above $Re = 150$, the secondary shedding region of the wake is no longer periodic. This is seen in Fig. 16 where the normalised power spectrum has many more frequency components, with the low frequency component still present. At $Re = 150$, after the primary frequency has decayed, there is only one dominant frequency in the far wake (Fig. 14). However, at $Re = 175$, three dominant frequencies are present (Fig. 16). There is a transition to lower frequencies as the flow structures

move downstream. Below $X/D \approx 12$, the primary frequency is due to the vortex shedding from the elliptical cylinder which has the most energy. Beyond $X/D \approx 12$, the primary vortices roll into each other due to the influence of the two-dimensional instability. Beyond $X/D \approx 70$, the tertiary frequency shown in Fig. 17 becomes the dominant frequency where the secondary vortex structures are rolling up into larger scale structures.

4. Conclusion

This paper has presented the power spectra of velocity along the centreline of wakes in the flow around an elliptical cylinder with varied *AR* and *Re* values. It has been shown that, as the *AR* is decreased and/or the *Re* is increased, low frequency two-dimensional structures appear in the far wake increasingly closer to the cylinder. The normalised power spectrum plots indicate that the flow structures are evolving into larger scale structures with associated lower frequencies.

These results indicate that an alternative explanation of the low frequency unsteadiness found in the 2D simulations by Najjar and Balachandar [1] is that it can be due to a two-dimensional instability that has been observed in the far wake [6] interacting with the vortices shed from the flat plate.

Similar to experimental results of Williamson and Prasad [9], a low frequency instability was found in simulations at high *Re* and/or low *AR*. In the experiments, the two-dimensional instability (F_T) was triggered by an external source which resulted in a constant value for the low frequency. However, in the simulations the low frequency was not constant and varied with *Re* and *AR*. In the F2NI and F2 regimes where a secondary frequency was present in the far wake, no low frequencies were found in the power spectrum analysis.

For $AR = 1$, (a circular cylinder) no secondary frequencies were observed in the wake. This is likely due to the fact that, for circular cylinders, secondary structures develop at over $100A$ downstream. This is in contrast to some experiments where secondary wake structures were observed for circular cylinder at smaller downstream distances [9]. However, in the experiments it was shown that the far wake was extremely sensitive to external disturbances. In the case of the present simulations, the far wake structures are not prematurely triggered by external noise and thus we obtain the natural state of far wake.

Using power spectra provides information about the characteristics of the wake structures beyond that garnered by flow visualisation. This makes it possible to clearly distinguish different regions of the parameter space model. Although it is possible to visualise the low frequency component of the wake, it was only identified and quantified after analysing the power spectrum. The inception point for the secondary frequency was found to occur at lower *Re* than previously considered; it was not seen in the lower *Re* flow visualisations because the vortices from the cylinder had decayed before the 2-dimensional instability grew significantly. However, visualisations are clearly useful to relate the frequencies back to the physical structures in the wake

Circular cylinders are used as the generic geometry for simulations of flows around bluff bodies. However, the associated wake structures only encompass a subset of wake structures associated with bluff bodies, at least within the first hundred diameters downstream. Other simple bluff body shapes should also be considered in order to fully understand the dynamics of bluff body wake dynamics.

Acknowledgements

The authors gratefully acknowledge the computing resources provided by VPAC and APAC for the numerical simulations and support from a Large Grant from the Australian Research Council.

References

[1] F.M. Najjar, S. Balachandar, Low-frequency unsteadiness in the wake of a normal flat plate, J. Fluid Mech. 370 (1998) 101–147.
[2] C.H.K. Williamson, Three-dimensional wake transition, J. Fluid Mech. 328 (1996) 345–407.
[3] C.H.K. Williamson, The natural and forced formation of spot-like 'vortex dislocations' in the transition of a wake, J. Fluid Mech. 243 (1992) 393–405.
[4] S. Taneda, Downstream development of wakes behind cylinder, J. Phys. Soc. Japan 14 (1959) 843–850.
[5] J.M. Cimbala, H.M. Nagib, A. Roshko, Large structures in the far wake of two-dimensional bluff bodies, J. Fluid Mech. 190 (1988) 265–298.
[6] C.H.K. Williamson, A. Prasad, Oblique wave interactions in the far wake, Phys. Fluids 5 (1993) 1854–1857.
[7] S.A. Johnson, M.C. Thompson, K. Hourigan, Flow past elliptical cylinders at low Reynolds numbers, in: 14th Australasian Fluid Mechanics Conference, Adelaide, 2001.
[8] M.C. Thompson, K. Hourigan, J. Sheridan, Three-dimensional instabilities in the wake of a circular cylinder, Exp. Therm. Fluid Sci. 12 (1996) 190–196.
[9] C.H.K. Williamson, A. Prasad, A new mechanism for oblique wave resonance in the 'natural' far wake, J. Fluid Mech. 256 (1993) 269–313.